Observed Propagation Route of VLF Transmitter Signals in the Magnetosphere

Zhenxia Zhang[1,2] (ID)**, Lunjin Chen**[2] (ID)**, Xinqiao Li**[3]**, Zhiyang Xia**[2] (ID)**, Roderick A. Heelis**[2] (ID)**, and Richard B. Horne**[4] (ID)

[1]Development Research Center of China Earthquake Administration, Beijing, China, [2]Department of Physics, University of Texas at Dallas, Richardson, TX, USA, [3]Institute of High Energy Physics, Chinese Academy of Sciences, Beijing, China, [4]British Antarctic Survey, Cambridge, UK

Correspondence to:
L. Chen,
Lunjin.Chen@gmail.com

Abstract Signals of powerful ground transmitters at various places have been detected by satellites in near-Earth space. The study on propagation mode, ducted or nonducted, has attracted much attentions for several decades. Based on the statistical results from Van Allen Probes (data from October 2012 to March 2017) and DEMETER satellite (from January 2006 to December 2007), we present the ground transmitter signals distributed clearly in ionosphere and magnetosphere. The observed propagation route in the meridian plane in the magnetosphere for each of various transmitters from the combination of DEMETER and Van Allen Probes data in nighttime is revealed for the first time. We use realistic ray tracing simulation and compare simulation results against Van Allen Probes and DEMETER observation. By comparison we demonstrate that the observed propagation route, with partial deviation from the field lines corresponding to ground stations, provides direct and clear statistical evidence that the nonducted propagation mode plays a main role, although with partial contribution from ducted propagation. The propagation characteristics of VLF transmitter signals in the magnetosphere are critical for quantitatively assessing their contribution to energetic electron loss in radiation belts.

Plain Language Summary The topic on signal propagation of ground-based VLF transmitter in ionosphere and magnetosphere has attracted much attention in several decades. But the question about the propagation mode (ducted or nonducted) has not been answered definitely due to lacks of direct support from statistical satellite data. In this paper, the observed propagation route in the meridian plane in the magentosphere for each of various transmitter from the combination of DEMETER and Van Allen Probes data is revealed for the first time. Based on satellite observation and ray tracing simulation, we provide a clear and strong proof that the nonducted mode of transmitter signal plays a main role. The determination of the propagation mode will play a significant role in many fields, including the wave propagation model development and electron population adjustment as radiation belt remediation, which aims at lowering the damage of relativistic particles to the spacecraft and astronaut.

1. Introduction

Ground-based VLF transmitters have been utilized for long-distance communication and geo-location in past decades (Swanson, 1983; Watt, 1967) and can penetrate through the ionosphere and propagate within the plasmasphere. The related ionosphere disturbances, particle precipitation, wisp electron precipitation structure (Sauvaud et al., 2008), heating phenomenon, and wave propagation have also been studied (Bell et al., 2011; Cohen & Inan, 2012; Gamble et al., 2008; Graf et al., 2009; Inan et al., 2007; Li et al., 2012; Marshall et al., 2010; Parrot et al., 2007, 2009; Starks et al., 2008; Tao et al., 2010).

For propagation in the plasmasphere, two theories of wave propagation have been proposed, ducted and nonducted. Sometimes, both can coexist. The former ducted mode requires the presence of density irregularities, which enables the signal well confined along the field line. Such mode is more favorable for whistler mode with frequency below than $f_{ce}/2$ (f_{ce} is electron cyclotron frequency; Smith et al., 1960; Smith, 1961). The nonducted mode does not require density irregularities. Instead, nonducted propagation takes place in a smoothly varying medium.

Table 1
VLF Transmitter Parameters Used in This Study

Call sign	Frequency (kHz)	Power (kW)	Geographic latitude (°)	Geographic longitude(°)	Geomagnetic latitude(°)	Geomagnetic longitude(°)
NWC	19.8	1000	−21.82	114.17	−31.46	187.31
NPM	21.4	600	21.42	201.85	21.83	270.55
NAA	24.0	1000	44.65	292.72	54.32	6.46
DHO	23.4	500	53.08	7.61	53.63	93.28
GQD	19.6	500	54.9	356.73	57.21	83.42
HWU	18.3	400	46.71	1.25	48.56	84.31
NDT	22.27		32.00	130.82	23.06	201.44
NTS	18.6		38.47	146.93	−45.66	225.44
NLK	24.8	250	48.20	238.08	53.91	300.83
NLM	25.2	500	46.37	261.67	54.91	328.53

Cerisier (1974) demonstrated both ducted and nonducted modes from magnetospheric observation of artificial VLF waves, with only the latter mode below $L \sim 1.7$. Clilverd et al. (2008) presented evidence to confirm the nonducted propagation in the plasmasphere at low L (< 1.5) but claimed the transmitter signals become highly ducted in the plasmasphere at higher L shell. These were based on the evidence that the power in conjugate region locates below $f < f_{ce}/2$, that is, there is a lack of significant wave power above $f_{ce}/2$. However, the satellite observation also presents the evidence that some VLF transmitter signals has exceeded the half gyroresonance frequency limit of ducted propagation (Foster et al., 2016; Ma et al., 2017).

For nonducted mode, Cerisier (1974) noted that for low-latitude transmitters (with $L < 1.9$), the final latitude in the conjugate hemisphere tends to be greater than the initial one, while for transmitters at higher latitudes (with $L > 1.9$), there are less changes between the initial and final latitude values. Because of this, only looking at the comparison between initial and final L values at a fixed ionospheric altitude cannot differentiate the propagation mode, ducted or nonducted, and therefore, different conclusions have been obtained. There has been ample past work on observational evidence of coexisting ducted and nonducted propagation, including the conjugate ground observation of the NAA transmitter signals (e.g., Clilverd, Smith, et al., 1992; Clilverd, Thomson, et al., 1992; Clilverd et al., 2008) and of VLF transmitter at Siple Station (e.g., Helliwell & Katsufrakis, 1974; Helliwell, 1988). Despite simulation efforts of magnetospheric propagation and comparative studies of ionospheric and magnetospheric signals of VLF transmitters in the past, a better understanding of propagation route of VLF transmitter signals in the magnetosphere can be obtained by combining statistical observation of the signals from Van Allen Probes with propagation simulation in a more realistic magnetic field model than a dipole field for such low L shells.

The determination of wave propagation, in particular, the variation of wave normal angles, for VLF transmitters is necessary for the quantification of the contribution of VLF transmitters in radiation belt electron loss (Bortnik et al., 2006; Gamble et al., 2008; Kulkarni et al., 2008; Rodger et al., 2010). Van Allen Probes with elliptic orbits provides an opportunity to investigate the propagation characteristics of ground transmitters from the ionosphere to the magnetosphere. Here we show propagation routes constructed directly from the observation, and also reproduce the propagation routes by ray tracing simulation.

2. Observations

2.1. Introduction of Transmitter Signals and Satellite Data

The ground-based VLF transmitters distributed all over the world in the frequency range of 18−41 kHz has been outlined in the work of Parrot et al. (2009). Here we list the main parameters in Table 1.

The low-altitude-orbiting DEMETER satellite (operating over 2005−2010) measures wave electric and magnetic fields (Berthelier et al., 2006; Lagoutte et al., 2006; Sauvaud et al., 2006). There are two data products of electric power spectral density, one measuring the VLF wave from 78 Hz to 20 kHz with frequency resolution 19.5 Hz, labeled as 1132 application process identifier (APID) in the level-1 data, and the other one in the HF range from 13 kHz to 3.3 MHz with frequency stepping 3.26 kHz, labeled as APID 1134.

The Van Allen Probes orbit (Mauk et al., 2013; operating since 2012) allows the spacecraft to continuously monitor the region of space covering a large range of altitude including near the Earth where the VLF

Table 2
The Frequency and Geomagnetic Longitude Ranges for Each VLF Transmitter Signals Measured by Satellites Used in This Work

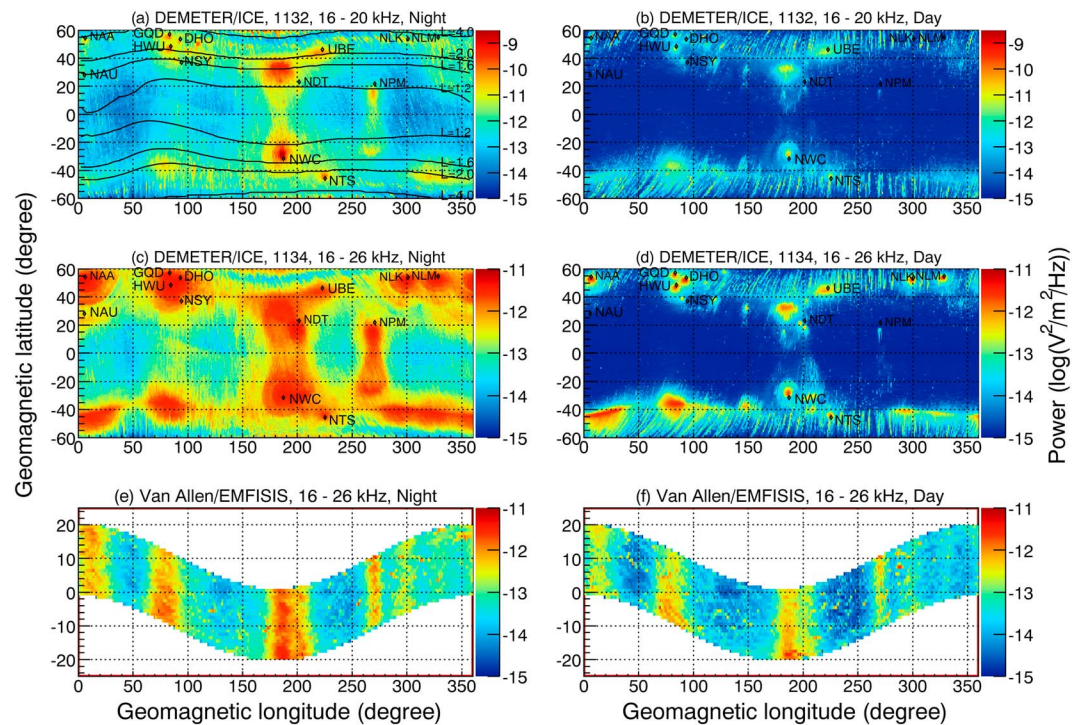| | DEMETER | | | | | | | Van Allen Probes | |
Call sign	Frequency (kHz)	Longitude (°)	Data type	λ_{peak} (°)	λ_{Nb} (°)	λ_{Sb} (°)	λ_{conj} (°)	Frequency channel (Hz)	Longitude (°)
NWC	19.59–19.98	180–195	1132 APID	−28.00	−26.25	−30.67	32.41	19573	180–195
GQD	19.39–19.79	78–88	1132 APID	55.00	57.36	53.44	−37.77	19573	65–85
HWU	18.11–18.50	78–88	1132 APID	46.00	48.73	44.21	36.5	18657	70–90
NTS	18.42–18.81	222–228	1132 APID	−44.00	−42.14	−45.83	44.57	18657	210–240
DHO	22.78–26.04	88–99	1134 APID	51.00	57.88	41.86	−38.04	23714	77–90
NPM	19.53–22.78	266–274	1134 APID	16.00	21.17	−11.45	−27.16	21544	264–276
NDT	19.53–22.78	197–205	1134 APID	18.00	24.99	6.66	−31.41	22603	195–212
NAA	22.78–26.04	355–16	1134 APID	50.00	59.15	35.89	−43.53	23714	0–20
NLK	22.78–26.04	294–304	1134 APID	51.00	56.82	42.54	−40.63	24879	294–306
NLM	22.78–26.04	322–332	1134 APID	54.00	58.44	43.75	−42.89	24879	322–334

ground-based transmitter signals are expected. Electromagnetic waves are measured by the Electric and Magnetic Field instrument Suite and Integrated Science (EMFISIS) waves instrument (Kletzing et al., 2013). For VLF transmitter signal observation, we use the high-frequency receiver instrument of EMFISIS, which measures spectra of one component of the wave electric field in the plane perpendicular to the spacecraft spin axis. The observed spectra from high-frequency receiver are collected every ~6 s and cover 82 logarithmically spacing frequency bins over the frequency range 10–400 kHz.

After visual inspection of the wave measurement month by month over the corresponding magnetic longitude range and over wave frequency range for the VLF ground transmitters (listed in Table 2) during the period from October 2012 to March 2017, we have confirmed that all the transmitters (except NTS) listed in Table 1 have been broadcasting for that entire duration.

2.2. Global Map of VLF Transmitter Signal

A global map of the wave intensity measured by the VLF and HF electric field instrument on board DEMETER satellite in geomagnetic coordinates is shown in Figures 1a–1d. The data used include survey and burst mode over the 2-year period from January 2006 to December 2007. For data analysis below, we have excluded the data in the magnetic longitude range (170°–210°) and the latitudinal range (−45° to 45°) near the NWC station during the months from July 2007 to December 2007 when the station turned off. The wave intensity is averaged in each of the (1°, 1°) pixels along the geomagnetic latitude and longitude. Each pixel of Panels (a) and (b) corresponds to APID 1132 data averaged over the frequency range between 16 and 20 kHz for daytime and nighttime, respectively. Panels (c) and (d) show wave intensity distribution from APID 1134 data averaged over the frequency range between 16 and 26 kHz. A quasi Sun-synchronous orbit of DEMETER, with the descending node at 10:30 LT and the ascending node at 22:30 LT, enables separation of data during daytime and nighttime. The enhancement of wave intensity in local and conjugate hemispheres at DEMETER altitude corresponding to each transmitter station listed in Table 1 can be apparently observed in the map, and the transmitter positions are tagged with little black dots. The L-shell values have been labeled as black lines in the panels from 1.2 to 4.0. We can find that there exists an obvious offset in L-values for the signal peaks at the DEMETER altitude between the southern and northern hemispheres (for example, NWC). Additionally, the diffraction ring pattern phenomenon (for example, Figure 1c) can be seen in the NAA, NLK, and NLM signals in local transmitter hemisphere, which is similar to the reported NWC diffraction pattern (Sauvaud et al., 2008).

In order to investigate the response of the transmitter signals in the magnetosphere, we sort VLF wave spectral density measured by EMFISIS instrument on board Van Allen Probes over the time period of October 2012 to March 2017 below altitude 13,000 km into 200 geomagnetic latitude bins of equal spacing from −90° to 90° and 200 geomagnetic longitude bins of equal spacing from 0° to 360°. The data are also sorted into the nighttime (MLT: 18:00 to next 6:00) and daytime (MLT: 6:00–18:00) maps, respectively, shown in Figures 1e and 1f. The shown power spectral density has been averaged over the frequency range from 18,657 to 24,879 Hz (seven frequency channels from EMFISIS measurement). Bursty lightning-generated whistlers, which are a

Figure 1. Global map of average wave power spectral density. Distributing in the geomagnetic latitude and longitude bins over the frequency range 16–20 kHz observed by DEMETER ICE APID 1132 (top), over the frequency range 16–26 kHz observed by DEMETER ICE APID 1134 (middle), and over 16–26 kHz from Van Allen Probes (bottom) during nighttime (left) and daytime (right). APID stands for application process identifier. DEMETER data over January 2006 to December 2007 and Van Allen Probes data over October 2012 to March 2017 are used. Ground transmitter locations are also marked as black dots. The black solid lines in (a) denote the contours of L-shell values.
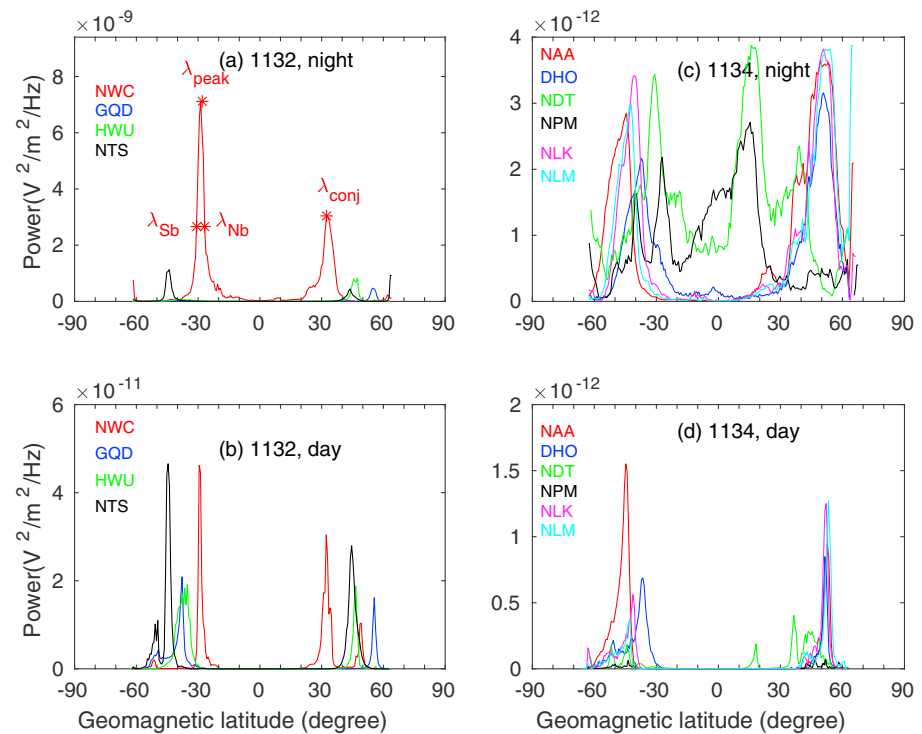
potential source of error for transmitter signal data analysis, are expected to contribute little because several years' data are averaged in each bin of geomagnetic latitude and longitude.

The emission signals from ground-based VLF transmitter stations NAA, NWC, NDT, NPM, NLK, and NLM are all obviously visible as localized peaks on the wave power map constructed from Van Allen Probes data (Figures 1e and 1f). Signals from GQD, HWU, and DHO stations, which are too close to see individual peaks, mix together and appear as a single broad peak in the averaged wave power. Nevertheless, the three stations, which have different operating frequencies (see Table 1), can be distinguished by selecting different frequency ranges.

2.3. 2-D Signal Distribution in Geomagnetic Latitude

Figure 2 shows the wave intensity distribution in the ionosphere measured by DEMETER as a function of geomagnetic latitudes. Narrow longitude and frequency ranges for each transmitter signal (shown in Table 2) are selected to reduce the DEMETER signal contamination from the bad anti-aliasing filter problem. The selected data are sorted into the bins of geomagnetic latitudes with equal spacing of 1° from −90° to 90° and then averaged in each bin to obtain the latitudinal distribution. The selected longitude ranges for each transmitter signal can be slightly different between the DEMETER and Van Allen Probes, due to azimuthal propagation especially at the presence of azimuthal density gradient (Clilverd et al., 2008; Clilverd, Smith, et al., 1992; Clilverd, Thomson, et al., 1992). In order to exhibit more accurately the wave intensity value in the local hemisphere regions and the conjugate hemisphere regions detected by satellite, we utilize the VLF electric field data (1132 APID data) with a higher frequency resolution to produce the wave intensity distribution for the stations with frequency below 20 kHz. Due to the 20-kHz upper limit of VLF electric field frequency, we have to use the HF electric field data (1134 APID data) to produce intensity distributions for the stations with frequency larger than 20 kHz. In summary, the wave intensity distribution for stations NWC, GQD, HWU, and NTS are produced from 1132 APID data, and the others left in the figure are from 1134 APID data. For a given station, the wave intensity from 1132 APID data (the left panels) is relatively high by about 3 orders of magnitude

Figure 2. The geomagnetic latitude distribution of wave power spectral density of VLF ground transmitter signals measured by DEMETER satellite during nighttime (top panels) and daytime (bottom panels). (a and b)1132 APID data with higher-frequency resolution, for NWC, GQD, HWU, and NTS signals with frequency below 20 kHz; (c and d) 1134 APID data with lower-frequency resolution, for NAA, DHO, NDT, NPM, NLK, and NLM signals with frequency above 20 kHz.
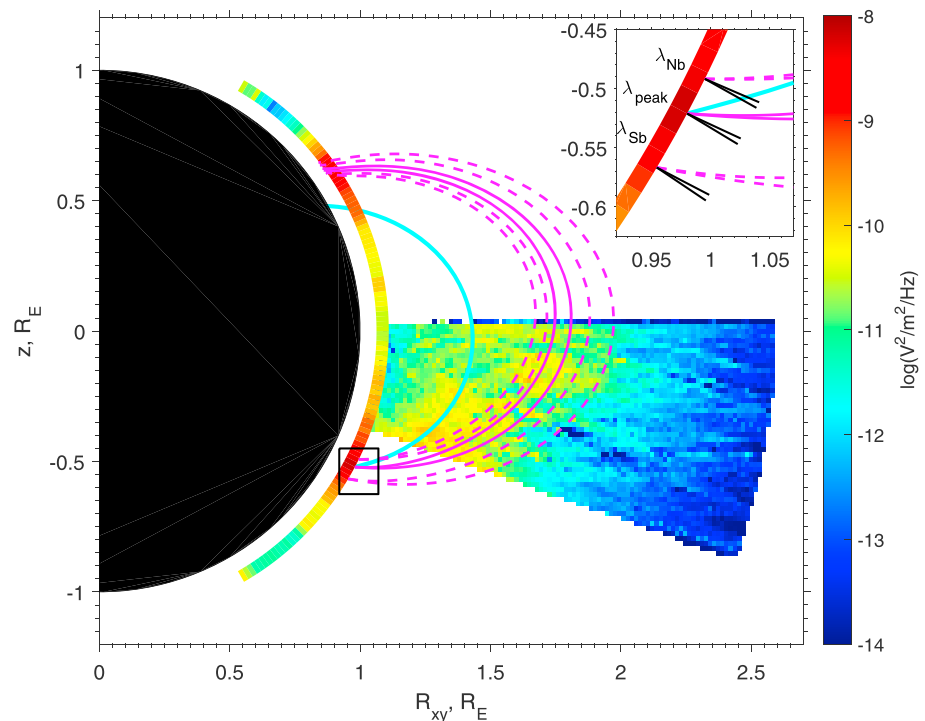
than that from 1134 APID data (the right panels) at nighttime. This is mainly because that the former intensity is obtained by average on a narrower frequency range, and the latter are obtained by averaging over a wider frequency range, which includes a larger percentage of background signals.

From Figure 2, we can see that there generally exists a pair of peaks for ground transmitter signal intensity, one at latitude of the source hemisphere (λ_{peak}), where a transmitter locates, and the other in the conjugate hemisphere (λ_{conj}). One can also see that the peaks at the source hemisphere have finite extension over the magnetic latitude, which can be denoted by the northward (λ_{Nb}) and southward (λ_{Sb}) boundaries, where the signal intensity is dropped by a factor of $1/e$ compared with the corresponding peak intensity. The obtained characteristic latitudes are listed in Table 2 and will be used as the input parameters for ray tracing simulation described in the next section. We can find that the NWC, NDT, and NPM signals with the lower latitude of transmitter stations propagate poleward into the conjugate hemisphere, while the signals of DHO, GQD, HWU, NAA, NLK, and NLM with higher latitude of stations propagate equatorward.

When comparing the signal intensity maps from DEMETER satellite at a fixed altitude in the ionosphere and the Van Allen Probes orbiting near the equatorial region in the magnetosphere, we identify well the signals from the same ground transmitters according to their geomagnetic longitude and operating frequencies (see Table 2). So we will combine the two satellite data sets to display the propagation profile in the meridian plane and then utilize the ray tracing model to simulate the propagation path, which can be directly compared against the observed path.

3. Ray Tracing Simulation

Through combination of observed data from DEMETER and Van Allen Probes, we present the propagation route of NWC signal in two-dimensional meridian plane, shown in Figure 3. The meridian distribution of the transmitter signal is obtained by (1) projecting all the observed data corresponding to the NWC transmitter frequency within a range of magnetic longitude (given by Table 2) centered near the station into the meridian plane by keeping the radial distance invariant, (2) sorting them into 2-D bins of 200 equally spacing $R_{xy}(= \sqrt{(x^2 + y^2)})$ from 0 to 2.6 R_E and 200 equally spacing z from -1.9 to $+1.9$ R_E, where x, y, and z are in

Figure 3. Comparison of NWC signals from the combined DEMETER (1132 APID) and Van Allen Probes observations in nighttime with the ray tracing simulation in the meridian plane. The cyan line represents International Geomagnetic Reference Field magnetic field line passing the location of the power peak of observed NWC signal from DEMETER. Two magenta solid lines denote ray paths originating from that location with initial wave normal directions at the edges of the transmission cone. Another two pairs of magenta dashed lines denote ray paths originating from two other locations, respectively, corresponding to the two latitudes with DEMETER-observed wave intensity $1/e$ of the peak intensity. Zoom-in plot of the black rectangular area illustrates the three locations above and corresponding transmission cones (denoted by pairs of black lines).

geomagnetic coordinates, and then (3) evaluating averaged power spectral density within each bin. The signal in conjugate hemisphere is shifted poleward across magnetic field lines, and in the magnetosphere gradually deviates from the original field line (in cyan) corresponding to the peak intensity at DEMETER altitude. As the signal reaches the equator, such deviation increases by 0.5 R_E from the original field line. At the conjugate hemisphere, the signal observed from DEMETER altitude ends by deviation 4.4° (32.4° – 28.0°) in magnetic latitude north of the conjugate foot point of the original field line. Such observed propagation path clearly demonstrates the nature of nonducted propagation.

To verify the nonducted propagation route, we simulate the NWC signal by ray tracing solver HOTRAY code (Horne, 1989), with initial setup according to the DEMETER measurement at the southern hemisphere, where the station is located, shown in Figure 3. The HOTRAY code is a ray tracing solver for electromagnetic and electrostatic wave propagation in a magnetized plasma medium, which has been extended to allow arbitrary magnetic field models and plasma density models. For near-Earth geospace medium of interest, we adopt a diffusive equilibrium plasma density model (Bortnik et al., 2011, and references within), where the ionospheric density peak of ∼10^6 cm^{-3} remains at an altitude of 250 km and the plasmapause is set to a typical L = 4.5 with a widthof0.3 R_E (R_E is the Earth radius). For the background magnetic field model, we used International Geomagnetic Reference Field (IGRF; Thébault et al., 2015), which is a more realistic representation than a dipole magnetic field for the region of interest. Given limited azimuthal spread of transmitter signals (Figure 1), we adopt 2-D ray tracing simulation in the meridian plane for simplicity.

Constrained from the observation, wave frequency is set by operating frequency of NWC station (=19.8 kHz). For the selection of an initial ray location, we use the DEMETER signal peak location for the corresponding VLF transmitter, denoted by its magnetic latitude λ_{peak}. Such latitude is slightly different from the magnetic latitude of NWC transmitter on the ground, because of subionospheric propagation. For choice of initial wave normal vectors, we work out the transmission cone for that location, within which the signal can transmit from

below the ionosphere to above. The transmission cone is aligned near the vertically upward direction and is of narrow angular width (typically several degrees), depending on VLF transmitter frequencies and the launch locations and a typical electron number density in nighttime E layer, which is set to a typical value 5×10^4 cm^{-3} (Helliwell, 1965, p. 65). The calculated transmission cone is used to determine two initial wave normal vectors, one northmost pointing and one southmost pointing in that meridian plane.
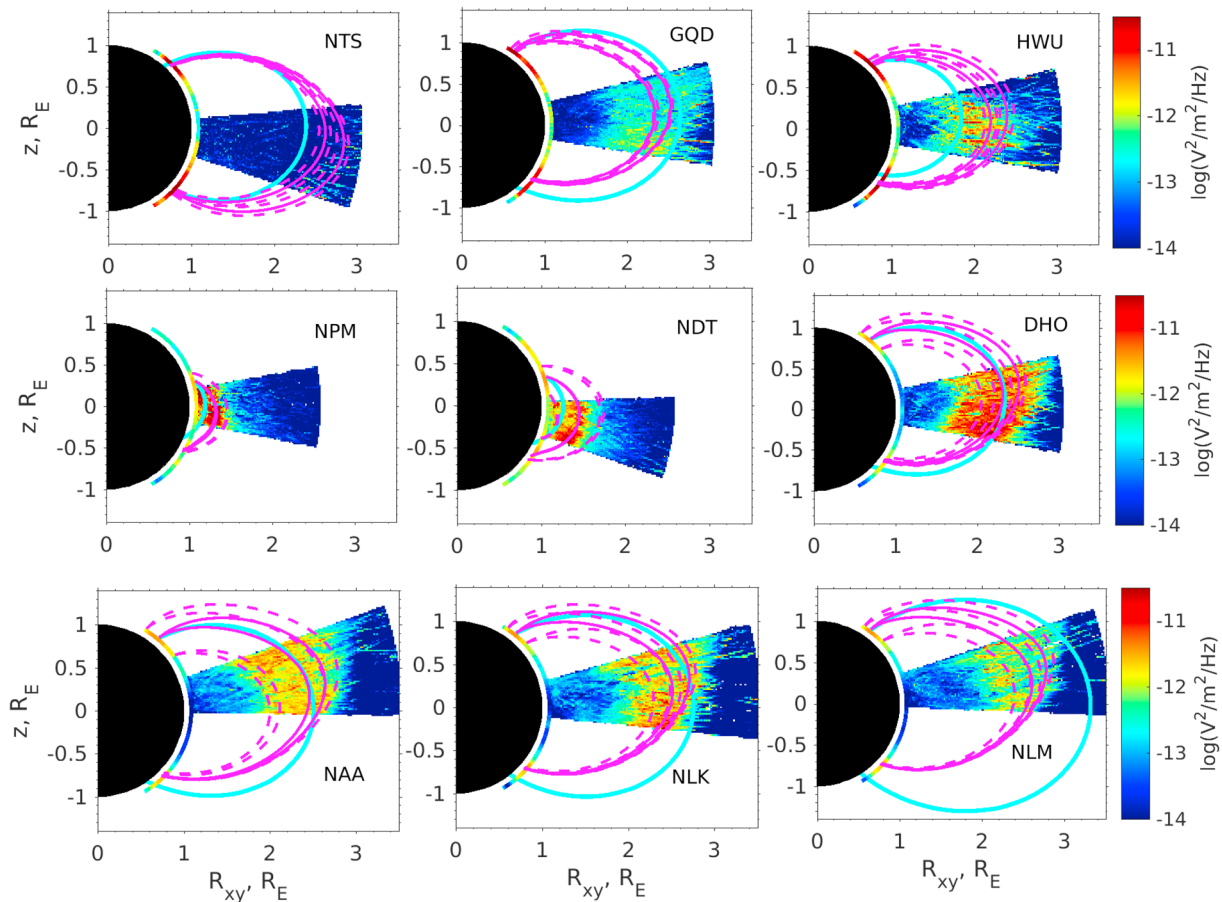
The simulated ray paths are shown as the two magenta solid lines, the region enclosed by which denotes the propagation spread originating from the signal peak with a finite size of transmission cone. According to DEMETER observation (see Figure 2), the signal at the DEMETER altitude is an extended source instead of a single point source, because of signal spread during the subionospheric waveguide propagation between the Earth and the ionosphere. The spatial extension can be approximated by the region of DEMETER-observed signal intensity demarcated by the two boundaries, northern and southern latitude (λ_{Nb} and λ_{Sb}), beyond which the signal intensity drops below $1/e$ of the peak intensity. For considering the extended source, we perform ray tracing simulation for rays launched at each of the two boundary locations with two initial wave vectors at the edges of the corresponding transmission cones. Their corresponding ray trajectories originating from the two boundaries are denoted by two pairs of dashed magenta lines, respectively. The region covered by the four dashed lines denotes propagation path spread over the spatially extended signal source from DEMETER altitude for NWC station. For NWC station in Figure 3, the two magenta solid lines, representing the paths from the power peak in the southern ionosphere, trace well partly with the route of intense NWC signal in the magnetosphere observed from Van Allen Probes. The spreading of signal energy near the original field line is also captured by the magenta dashed lines, which may be due to the finite extent of the signal source in the DEMETER altitude. In addition, the ray tracing also predicts accessing points at the conjugate hemisphere at the DEMETER altitude. The agreement between the combined DEMETER and Van Allen Probes signal distribution with ray tracing simulation provides strong proof that NWC station signal mainly follows the nonducted mode. We also note that some signal power can be close to the original field line near the transmitter location, which suggests the coexistence of propagation in ducted mode. This is consistent with the findings of Cohen et al. (2012). However, we did not find the corresponding power peak at the conjugate point of the same field line, which supports the nonducted mode as primary propagation mode.

We also perform similar simulations for nine other stations and compare with observations in Figure 4. For the observed wave distribution on the meridian plane, different upper limits of R_{xy} are used to account for different altitude profiles for different stations. The upper limit is set to 2.6 R_E for NPM and NDT (the same as NWC); to 3.1 R_E for NTS, GQD, HWU, and DHO; and to 3.5 R_E for NAA, NLK, and NLM. We make the following notes for characteristics of whistler mode propagation in the magnetosphere to understand the ray tracing results as noted previously by Cerisier (1974).

- The curvature of magnetic field lines tends to refract wave normal direction outward.
- For the outward wave vectors, the group velocity has outward component for frequency $f < 1/2f_{ce}$ and has inward component for $f > 1/2f_{ce}$.
- Since VLF is generally above lower hybrid resonance frequency, no magnetospheric reflection takes place.

The agreement between observation and simulation for all stations are also seen in Figure 4 except NTS station, which is turned off in 2008 and only can be observed by DEMETER. First, signal from stations at low latitudes (NPM, NDT, and HWU) propagates outward, because wave frequency stays below $f_{ce}/2$ at such low L shell. Second, signal from stations at high latitudes (GQD, DHO, NAA, NLK, and NLM) experiences a net inward propagation from the hemisphere where stations locate to the conjugate hemisphere; most of inward propagation takes place near the equatorial region where f/f_{ce} exceeds 1/2 and becomes highest at the equator. The fine differences between simulation and observation may be due to (1) the simplified density model used without local time dependence and (2) the extended width estimate of signal at DEMETER altitude is not accurate enough when the DEMETER signal falls off slowly with latitudes away from the peak, for example, NPM in Figure 2c. We also note that the use of IGRF magnetic field is necessary to account for the observation due to the effect of South Atlantic Anomaly region, especially for GQD, HWU, and DHO stations.

Finally, we note that to determine the primary propagation mode, one should compare the power variation envelope in the 2-D meridian plane with the coverage of ray paths from the transmitter source at DEMETER over a finite latitude extent and over a finite wave normal angle range (represented by magenta lines in Figures 3 and 4). When a signal is observed by satellites at the field line connecting to a transmitter, it does not mean the propagation mode is ducted. It can be as well due to nonducted propagation of a signal source

Figure 4. Comparison of nine other ground transmitter signals from the combined DEMETER and Van Allen Probes observations in nighttime with the corresponding ray tracing simulation in a similar format to Figure 3 (for NWC).

over the finite latitude extent in the ionosphere and over a finite wave normal angle range. Some disagreement for GQD and HWU stations in Figure 4 is noted. This may be due to the fact that the two stations are at close magnetic longitudes (83.4° for GQD and 84.3° for HWU) and have close operating frequency (19.6 kHz for GQD and 18.3 kHz for HWU), which leads to some degree of data corruption in the analysis.

Here we summarize the propagation mode for VLF transmitters considered in this work. For NTS, which has been turned off before Van Allen Probes launch, no signal is detected by them, which is just a good confirmation that the EMFISIS observations indeed correspond to VLF transmitter signals. DEMETER results alone suggest both ducted and nonducted propagation. For GQD, HWU, and DHO, it seems that both ducted and nonducted propagations are effective in illuminating the near-equatorial and conjugate regions. But obviously, nonducted propagation is needed to explain magnetospheric signals. For NPM, EMFISIS results correspond well to ducted and partially to nonducted propagation. For NDT, both DEMETER and EMFISIS illumination correspond to nonducted. For NAA, NLK, and NLM, both the radially deep region of illumination observed by EMFISIS and conjugate signal by DEMETER need the explanation by nonducted propagation.

4. Conclusion

In sum, we combine the observation from DEMETER satellite and Van Allen Probes and display the propagation contour of ground-based VLF transmitters in the ionosphere and magnetosphere. The NWC, NDT, and NPM signals with the lower latitude of transmitter stations propagate poleward into the conjugate hemisphere. While the signals of DHO, GQD, HWU, NAA, NLK, NLM, and NTS with higher latitude of stations propagate equatorward. Although this propagation characteristics of VLF ground transmitter signal has been investigated previously (Kulkarni et al., 2008), our ray tracing simulation has greater advantages in the

following three aspects: (1) we use observed sources instead of hypothetical sources, (2) a more realistic IGRF field than a dipole magnetic field is adopted, and (3) direct comparison with observation is made. The agreement of propagation characteristics between satellite observation and ray tracing simulation provides direct and clear statistical evidence that the propagation of VLF ground-based transmitters in magnetosphere is dominated by nonducted mode. Understanding the distribution of VLF transmitter signals in the magnetosphere is critical for quantitatively assessing their contribution to energetic electron loss in radiation belts.

References

Bell, T. F., Graf, K., Inan, U. S., Piddyachiy, D., & Parrot, M. (2011). DEMETER observations of ionospheric heating by powerful VLF transmitters. *Geophysical Research Letters*, *38*, L11103. https://doi.org/10.1029/2011GL047503

Berthelier, J. J., Godefroy, M., Leblanc, F., Malingre, M., Menvielle, M., Lagoutte, D., et al. (2006). ICE, the electric field experiment on DEMETER. *Planetary and Space Science*, *54*, 456–471. https://doi.org/10.1016/j.pss.2005.10.016

Bortnik, J., Chen, L., Li, W., Thorne, R. M., & Horne, R. B. (2011). Modeling the evolution of chorus waves into plasmaspheric hiss. *Journal of Geophysical Research*, *116*, A08221. https://doi.org/10.1029/2011JA016499

Bortnik, J., Inan, U. S., & Bell, T. F. (2006). Temporal signatures of radiation belt electron precipitation induced by lightning-generated MR whistler waves: 2. Global signatures. *Journal of Geophysical Research*, *111*, A02205. https://doi.org/10.1029/2005JA011398

Cerisier, J. C. (1974). Ducted and partly ducted propagation of VLF waves through the magnetosphere. *Journal of Atmospheric and Terrestrial Physics*, *36*, 1443–1467.

Clilverd, M. A., Thomson, N. R., & Smith, A. J. (1992). Observation of two preferred propagation paths for whistler-mode VLF signals received at a non-conjugate location. *Journal of Atmospheric and Terrestrial Physics*, *54*, 1075–1079. https://doi.org/10.1016/0021-9169(92)90073-T

Clilverd, M. A., Smith, A. J., & Thomson, N. R. (1992). The effects of horizontal ionospheric electron-density gradients on whistler mode signals. *Journal of Atmospheric and Terrestrial Physics*, *54*, 1061–1074. https://doi.org/10.1016/0021-9169(92)90072-S

Clilverd, M. A., Rodger, C. J., Gamble, R., Meredith, N. P., Parrot, M., Berthelier, J. J., & Thomson, N. R. (2008). Ground-based transmitter signals observed from space: Ducted or nonducted? *Journal of Geophysical Research*, *113*, A04211. https://doi.org/10.1029/2007JA012602

Cohen, M. B., & Inan, U. S. (2012). Terrestrial VLF transmitter injection into the magnetosphere. *Journal of Geophysical Research*, *117*, A08310. https://doi.org/10.1029/2012JA017992

Foster, J. C., Erickson, P. J., Baker, D. N., Jaynes, A. N., Mishin, E. V., Fennel, J. F., et al. (2016). Observations of the impenetrable barrier, the plasmaspause, and the VLF bubble during the 17 March 2015 storm. *Journal of Geophysical Research: Space Physics*, *121*, 5537–5548. https://doi.org/10.1002/2016JA022509

Gamble, R. J., Rodger, C. J., Clilverd, M. A., Sauvaud, J. A., Thomson, N. R., Stewart, S. L., et al. (2008). Radiation belt electron precipitation by man-made VLF transmissions. *Journal of Geophysical Research*, *113*, A10211. https://doi.org/10.1029/2008JA013369

Graf, K. L., Inan, U. S., Piddyachiy, D., Kulkarni, P., Parrot, M., & Sauvaud, J. A. (2009). DEMETER observations of transmitter-induced precipitation of inner radiation belt electrons. *Journal of Geophysical Research*, *114*, A07205. https://doi.org/10.1029/2008JA13949

Helliwell, R. (1988). VLF Wave injection experiments from Siple Station. *Advances in Space Research*, *8*(1), 279–289.

Helliwell, R. A. (1965). *Whistlers and related ionospheric phenomena*. Stanford University Press.

Helliwell, R. A., & Katsufrakis, J. P. (1974). VLF wave injection into the magnetosphere from Siple Station, Antarctica. *Journal of Geophysical Research*, *79*(16), 2511–2518.

Horne, R. B. (1989). Path-integrated growth of electrostatic waves: the generation of terrestrial myriametric radiation. *Journal of Geophysical Research*, *94*(A7), 8895–8909. https://doi.org/0148-0227/89/89JA-00197$\$05.00

Inan, U. S., Golkowski, M., Casey, M. K., Moore, R. C., Peter, W., Kulkarni, P., et al. (2007). Subionospheric VLF observations of transmitter-induced precipitation of inner radiation belt electrons. *Geophysical Research Letters*, *34*, L02106. https://doi.org/10.1029/2006GL028494

Kletzing, C. A., Kurth, W. S., Acuna, M., MacDowall, R. J., Torbert, R. B., Averkamp, T., et al. (2013). The Electric and Magnetic Field Instrument Suite and Integrated Science (EMFISIS) on RBSP. *Space Science Reviews*, *179*, 127–181. https://doi.org/10.1007/s11214-013-9993-6

Kulkarni, P., Inan, U. S., Bell, T. F., & Bortnik, J. (2008). Precipitation signatures of ground-based VLF transmitters. *Journal of Geophysical Research*, *113*, A07214. https://doi.org/10.1029/2007JA012569

Lagoutte, D., Brochot, J. Y., Carvalho, D. D., Elie, F., Harivelo, F., Hobara, Y., et al. (2006). The DEMETER science mission centre. *Planetary and Space Science*, *54*, 428–440. https://doi.org/10.1016/j.pss.2005.10.014

Li, X. Q., Ma, Y. Q., Wang, P., Wang, H. Y., Lu, H., Zhang, X. M., et al. (2012). Study of the North West Cape electron belts observed by DEMETER satellite. *Journal of Geophysical Research*, *117*, A04201. https://doi.org/10.1029/2011JA017121

Ma, Q., Mourenas, D., Li, W., Artemyev, A., & Thorne, R. M. (2017). VLF Waves from ground-based transmitters observed by the Van Allen Probes: Statistical model and effects on plasmaspheric electrons. *Geophysical Research Letters*, *44*, 6483–6491. https://doi.org/10.1002/2017GL073885

Marshall, R. A., Newsome, R. T., Lehtinen, N. G., Lavassar, N., & Inan, U. S. (2010). Optical signatures of radiation belt electron precipitation induced by ground-based VLF transmitters. *Journal of Geophysical Research*, *115*, A08206. https://doi.org/10.1029/2010JA015394

Mauk, B. H., Fox, N. J., Kanekal, S. G., Kessel, R. L., Sibeck, D. G., & Ukhorskiy, A. (2013). Science objectives and rationale for the Radiation Belt Storm Probes mission. *Space Science Reviews*, *179*, 3–27. https://doi.org/10.1007/s11214-012-9908-y

Parrot, M., Inan, U. S., Lehtinen, N. G., & Pincon, J. L. (2009). Penetration of lightning MF signals to the upper ionosphere over VLF ground-based transmitters. *Journal of Geophysical Research*, *114*, A12318. https://doi.org/10.1029/2009JA014598

Parrot, M., Sauvaud, J. A., Berthelier, J. J., & Lebreton, J. P. (2007). First in-situ observations of strong ionospheric perturbations generated by a powerful VLF ground-based transmitter. *Geophysical Research Letters*, *34*, L11111. https://doi.org/10.1029/GL029368

Rodger, C. J., Carson, B. R., Cummer, S. A., Gamble, R. J., Clilverd, M. A., Green, J. C., et al. (2010). Contrasting the efficiency of radiation belt losses caused by ducted and nonducted whistler-mode waves from ground-based transmitters. *Journal of Geophysical Research*, *115*, A12208. https://doi.org/10.1029/2010JA015880

Sauvaud, J. A., Maggiolo, R., Jacquey, C., Parrot, M., Berthelier, J. J., et al. (2008). Radiation belt electron precipitation due to VLF transmitters: Satellite observations. *Geophysical Research Letters*, *35*, L09101. https://doi.org/10.1029/2008GL033194

Sauvaud, J. A., Moreau, T., Maggiolo, R., Treilhou, J. P., Jacquey, C., Cros, A., et al. (2006). High-energy electron detection onboard DEMETER: The IDP spectrometer, description and first results on the inner belt. *Planetary and Space Science*, *54*, 502–511. https://doi.org/10.1016/j.pss.2005.10.019

Smith, R. L. (1961). Propagation characteristics of whistlers trapped in field-aligned columns of enhanced ionization. *Journal of Geophysical Research*, *66*(11), 3699–3707.

Smith, R. L., Helliwell, R. A., & Yabroff, I. W. (1960). A theory of trapping of whistlers in field-aligned columns of enhanced ionization. *Journal of Geophysical Research*, *65*(3), 40.

Starks, M. J., Quinn, R. A., Ginet, G. P., Albert, J. M., Sales, G. S., Reinisch, B. W., & Song, P. (2008). Illumination of the plasmasphere by terrestrial very low frequency transmitters: Model validation. *Journal of Geophysical Research*, *113*, A09320. https://doi.org/10.1029/2008JA013112

Swanson, E. (1983). Omega. *Proceedings of the IEEE*, *71*(10), 1140–1155.

Tao, X., Bortnik, J., & Friedrich, M. (2010). Variance of transionospheric VLF wave power absorption. *Journal of Geophysical Research*, *115*, A07303. https://doi.org/10.1029/2009JA015115

Thébault, E., Finlay, C. C., Beggan, C. D., Alken, P., Aubert, J., Barrois, O., et al. (2015). International Geomagnetic Reference Field: The 12th generation. *Earth Planets Space*, *67*, 79. https://doi.org/10.1186/s40623-015-0228-9

Watt, A. D. (1967). *VLF radio engineering*. UK: Pergamon Oxford.